30. R. Gersonde *et al.*, *Paleoceanography* **18**, 1061 (2003).
31. A. Shemesh, L. H. Burckle, J. D. Hays, *Science* **266**, 1542 (1994).
32. D. M. Sigman, E. A. Boyle, *Nature* **407**, 859 (2000).
33. I. R. Hall, I. N. McCave, N. J. Shackleton, G. P. Weedon, S. E. Harris, *Nature* **412**, 809 (2001).
34. C. D. Charles, S. J. Lynch, U. S. Ninnemann, R. G. Fairbanks, *Earth Planet. Sci. Lett.* **142**, 19 (1996).
35. P. G. Mortyn, C. D. Charles, U. S. Ninnemann, K. Ludwig, D. A. Hodell, *Geochem. Geophys. Geosyst.* **4**, 8405 (2003).
36. L. D. Stott, C. Poulsen, S. Lund, R. Thunell, *Science* **297**, 222 (2002).
37. N. J. Shackleton, *Pangaea*, http://doi.pangaea.de/10.1594/PANGAEA.58229 (2001).
38. T. Blunier, E. J. Brook, *Science* **291**, 109 (2001).
39. T. F. Stocker, *Science* **282**, 61 (1998).
40. H. Rashid, R. Hesse, D. J. W. Piper, *Paleoceanography* **18**, 1077 (2003).
41. J. F. McManus, D. W. Oppo, J. L. Cullen, *Science* **283**, 971 (1999).
42. G. Cortese, A. Abelmann, *Palaeogeogr. Palaeoclim. Palaeoecol.* **182**, 259 (2002).
43. A. P. S. Wong, N. L. Bindoff, J. A. Church, *Nature* **400**, 440 (1999).
44. R. Schlitzer, *Eos Trans. AGU* **81**, 45 (2000).
45. K. Speer, S. R. Rintoul, B. Sloyan, *J. Phys. Oceanogr.* **30**, 3212 (2000).
46. M. R. Chapman, N. J. Shackleton, *Geology* **27**, 795 (1999).
47. S. A. van Kreveld, M. Knappertsbusch, J. Ottens, G. M. Ganssen, J. E. van Hinte, *Mar. Geol.* **131**, 21 (1996).
48. R. N. Hiscott, A. E. Aksu, P. J. Mudie, D. F. Parsons, *Global Planet. Change* **28**, 227 (2001).
49. N. J. Shackleton, R. G. Fairbanks, T.-C. Chiu, F. Parrenin, *Quat. Sci. Rev.* **23**, 1513 (2004).
50. The sediment core for this study was obtained through the International Marine Global Change Studies (IMAGES) project. We thank the Institut Polaire Français Paul Emile Victor (IPEV) for technical support and for making the research vessel *Marion Dufresne* available for core retrieval. We are particularly indebted to Y. Balut and his team for their expert skills in designing and running the long Calypso piston corer. Financial support from the Deutsche Forschungsgemeinschaft contributed to the coring campaign. Special thanks go to G. Bianchi, Cardiff, for running the mass spectrometer and maintaining the high quality of data output. This work was supported by The Leverhulme Trust (UK) through grant F/407/J to R.Z. The data will be made available on the NOAA Paleoclimatology Web site (www.ngdc.noaa.gov/paleo/data.html) and in the PANGAEA database (www.pangaea.de).

Supporting Online Material
www.sciencemag.org/cgi/content/full/307/5716/1741/DC1
Materials and Methods
SOM Text
Figs. S1 to S5
References

30 June 2004; accepted 24 January 2005
10.1126/science.1102163

An Acylation Cycle Regulates Localization and Activity of Palmitoylated Ras Isoforms

Oliver Rocks,[1,3] Anna Peyker,[3] Martin Kahms,[1] Peter J. Verveer,[3] Carolin Koerner,[1] Maria Lumbierres,[2] Jürgen Kuhlmann,[1] Herbert Waldmann,[2] Alfred Wittinghofer,[1]* Philippe I. H. Bastiaens[3]*

We show that the specific subcellular distribution of H- and Nras guanosine triphosphate–binding proteins is generated by a constitutive de/reacylation cycle that operates on palmitoylated proteins, driving their rapid exchange between the plasma membrane (PM) and the Golgi apparatus. Depalmitoylation redistributes farnesylated Ras in all membranes, followed by repalmitoylation and trapping of Ras at the Golgi, from where it is redirected to the PM via the secretory pathway. This continuous cycle prevents Ras from nonspecific residence on endomembranes, thereby maintaining the specific intracellular compartmentalization. The de/reacylation cycle also initiates Ras activation at the Golgi by transport of PM-localized Ras guanosine triphosphate. Different de/repalmitoylation kinetics account for isoform-specific activation responses to growth factors.

Signaling networks are spatially organized by the specific localization of their protein constituents to distinct protein scaffolds, membrane systems, or microdomains. The three abundant Ras guanosine triphosphate–binding proteins Hras, Nras, and Kras4B (*1*, *2*) are a paradigm example of this spatial organization of signaling molecules. Although highly homologous and indistinguishable in most in vitro assays, these proteins have been shown to produce isoform-specific biological outputs, attributed to differences in plasma membrane (PM) and subcellular membrane localization. Their distribution is determined by different C-terminal lipid modifications. Posttranslationally modified Hras and Nras localize to the PM and to Golgi membranes, whereas Kras is apparently confined to the PM. The isoforms take different trafficking routes during posttranslational maturation. All isoforms undergo three steps of modification of the C-terminal CAAX motif (*3*), including farnesylation of the CAAX cysteine (*4*) in the cytosol, AAX proteolysis (*5*), and methylation of the farnesylated cysteine (*6*) on the endoplasmic reticulum (ER). Farnesylation alone cannot stably anchor proteins to lipid bilayers (*7*). Nras and Hras are further modified with palmitate moieties that are attached to one or two cysteines, respectively. Both fully posttranslationally modified isoforms access the PM from the surface of the ER via the secretory pathway (*8*, *9*). Kras bypasses the secretory pathway and exits the ER toward the PM without further lipid modification. A polybasic sequence near the C terminus allows stable interaction with anionic phospholipids at the inner leaflet of the PM. Unlike farnesylation, palmitoylation is reversible. The localization and mechanism of the latter lipid modification reaction in mammals is currently unclear, as both enzymatic and nonenzymatic processes are debated (*10*).

A long-held view has been that Ras only operates at the PM. Recent publications, however, have pointed out the importance of Ras compartmentalization for signal transduction (*11*, *12*). The Ras Golgi pool might represent a signaling entity separate from the PM, with distinct activation kinetics and signal propagation (*12*, *13*). Growth factor–induced Golgi Hras activation occurs independently of PM Hras and involves a pathway containing Src family kinases, phospholipase C-γ (PLCγ), and the Ras exchange factor RasGRP1 (*14*). A Golgi-resident mitogen-activated protein kinase scaffold (*15*), Sef, further supports this organelle as a signal platform. Yet it is unclear how cells achieve specific compartmentalized localization and regulate activity of palmitoylated Ras isoforms. Golgi Ras is believed to represent a trafficking intermediate of nascent protein en route to the PM, its ultimate target. However, considering the 1-day half-life of Ras (*16*) and exocytic transport on the time scale of 10 to 20 min (*17*), it is unlikely that a cell could uphold high Golgi Ras concentrations by the unidirectional transport model. Likewise, it is not clear how a cell prevents spillover of PM Ras to endomembranes, considering spontaneous intermembrane transfer (*18*) and continuous fusion and mixing of membranes (*19*). We show that the reversibility of palmitoylation is essential for maintaining specific localization of palmitoylated Ras isoforms to the PM and Golgi apparatus and has a role in the differential Ras isoform activity responses by regulating the partitioning between these compartments.

Rapid retrograde trafficking of palmitoylated Ras isoforms from the PM to the Golgi apparatus. Hras- or Nras-expressing cells were treated with a protein synthesis

[1]Department of Structural Biology, [2]Department of Chemical Biology, Max Planck Institute for Molecular Physiology, Otto-Hahn-Straβe 11, 44227 Dortmund, Germany. [3]European Molecular Biology Laboratory, Meyerhofstraβe 1, 69117 Heidelberg, Germany.

*To whom correspondence should be addressed. E-mail: alfred.wittinghofer@mpi-dortmund.mpg.de (A.W.) and bastiaen@embl.de (P.I.H.B.)

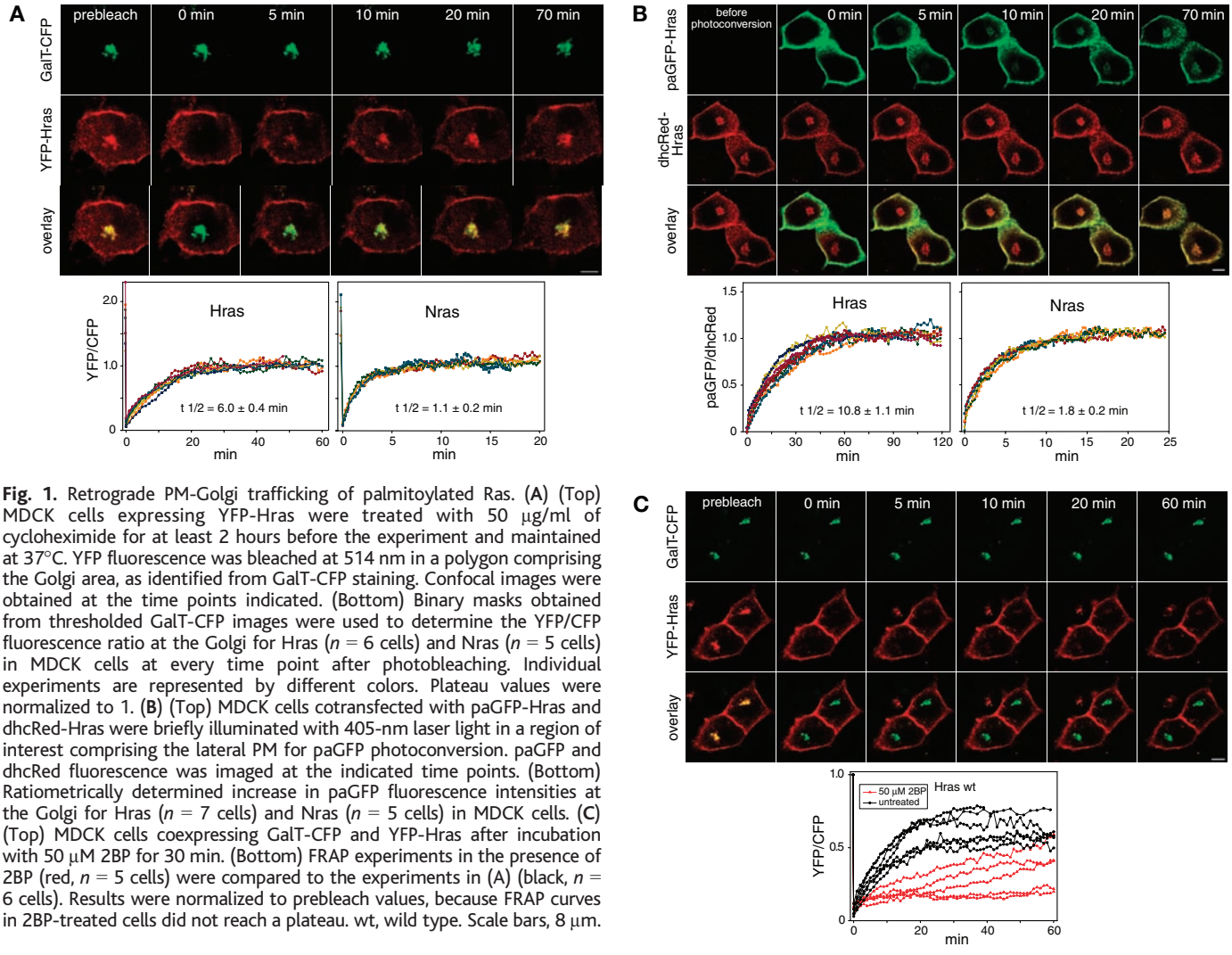

Fig. 1. Retrograde PM-Golgi trafficking of palmitoylated Ras. (**A**) (Top) MDCK cells expressing YFP-Hras were treated with 50 μg/ml of cycloheximide for at least 2 hours before the experiment and maintained at 37°C. YFP fluorescence was bleached at 514 nm in a polygon comprising the Golgi area, as identified from GalT-CFP staining. Confocal images were obtained at the time points indicated. (Bottom) Binary masks obtained from thresholded GalT-CFP images were used to determine the YFP/CFP fluorescence ratio at the Golgi for Hras (n = 6 cells) and Nras (n = 5 cells) in MDCK cells at every time point after photobleaching. Individual experiments are represented by different colors. Plateau values were normalized to 1. (**B**) (Top) MDCK cells cotransfected with paGFP-Hras and dhcRed-Hras were briefly illuminated with 405-nm laser light in a region of interest comprising the lateral PM for paGFP photoconversion. paGFP and dhcRed fluorescence was imaged at the indicated time points. (Bottom) Ratiometrically determined increase in paGFP fluorescence intensities at the Golgi for Hras (n = 7 cells) and Nras (n = 5 cells) in MDCK cells. (**C**) (Top) MDCK cells coexpressing GalT-CFP and YFP-Hras after incubation with 50 μM 2BP for 30 min. (Bottom) FRAP experiments in the presence of 2BP (red, n = 5 cells) were compared to the experiments in (A) (black, n = 6 cells). Results were normalized to prebleach values, because FRAP curves in 2BP-treated cells did not reach a plateau. wt, wild type. Scale bars, 8 μm.

inhibitor to chase nascent proteins out of the secretory pathway. In contrast to earlier reports (*8*, *9*), we observed extensive Golgi localization of both isoforms even after 12 hours of incubation with cycloheximide (fig. S1, A and B). Newly synthesized protein en route to the PM therefore does not solely account for Golgi-localized Ras. Fluorescence recovery after photobleaching (FRAP) experiments were performed to investigate if the Golgi Ras pool is a fraction of nascent protein that is temporally arrested at the Golgi during PM transport. Cells were transfected with the cyan fluorescent protein (CFP)–tagged Golgi marker GalT and either yellow fluorescent protein (YFP)–tagged Hras or Nras, then treated with cycloheximide. YFP fluorescence was then bleached at the Golgi, and the fluorescence recovery was determined ratiometrically (Fig. 1A). YFP-Hras Golgi fluorescence rapidly recovered with a half-time ($t_{1/2}$) of 6.0 ± 0.4 min in Madin-Darby canine kidney (MDCK) cells and 6.3 ± 0.3 min in COS-7 cells (fig. S2B). Because a substantial quantity of total Ras fluorescence was irreversibly photobleached at the Golgi, the extent of recovery depended on the relative Golgi volume of the individual cell observed. In COS-7 cells that have a much smaller relative Golgi volume, fluorescence recovery reached near-prebleach intensities, arguing against an immobilized fraction of Golgi Hras and suggesting an unhindered passage through this compartment. Reversibility of fluorescence as a cause of recovery at the Golgi could be ruled out, because YFP fluorescence recovered to not more than 3% of the initial intensity when the whole cell was bleached (*20*). Fluorescence recovery of monopalmitoylated YFP-Nras was almost six times faster than that of YFP-Hras, with a $t_{1/2}$ of 1.1 ± 0.2 min (Fig. 1A and fig. S2A). Thus, Golgi Ras is rapidly replenished by a protein pool present in the cell with kinetics that depend on the number of palmitoyl groups on the Ras isoforms.

To show that the Golgi pool is exchanged with protein from the PM, we fused a photoactivatable variant of green fluorescent protein (paGFP) (*21*) to Hras or Nras. paGFP-Hras or -Nras was selectively photoconverted at the lateral PM with 405-nm laser light, and accumulation of fluorescence was tracked at the Golgi. Coexpression of Ras fused to a tandem construct of *Heteractis crispa* hcRed (dhcRed-Ras), displaying correct subcellular localization and a minimized tendency to aggregate (*22*), allowed for ratiometric normalization of the photoproduct signal. Hras appeared at the Golgi with a $t_{1/2}$ of 10.8 ± 1.1 min (Fig. 1B), which is on the same time scale as that observed in the FRAP experiments. Similarly, retrograde trafficking of Nras occurred six times faster, with a $t_{1/2}$ of 1.8 ± 0.2 min (Fig. 1B). Palmitoylated Ras thus cycles between the PM and the Golgi, with a retrograde transport of PM-localized protein replenishing the Golgi pool. This transport is constitutive and independent of Ras activation state, because the same Golgi FRAP kinetics are seen in cells expressing oncogenic YFP-Hras G12V or dominant-negative YFP-Hras S17N (fig. S3A) that is no longer capable of interacting with downstream effectors.

A de/reacylation cycle is essential for specific PM or Golgi Ras localization. An

extensive set of experiments revealed that this retrograde trafficking is not mediated by clathrin coat–based endocytosis or by caveolae- or cholesterol-dependent endocytic mechanisms (supporting online text) (fig. S4, A to E). We therefore investigated if a sequence of depalmitoylation of Ras, redistribution to endomembranes, and repalmitoylation at the Golgi could account for the observed trafficking phenomenon, whereas spontaneous intermembrane transfer of dual lipid-anchored Ras peptides occurs on the order of hours (*18*), depalmitoylated Ras equilibrates in seconds between the aqueous and membrane phases (*23*), allowing rapid exchange between mem-

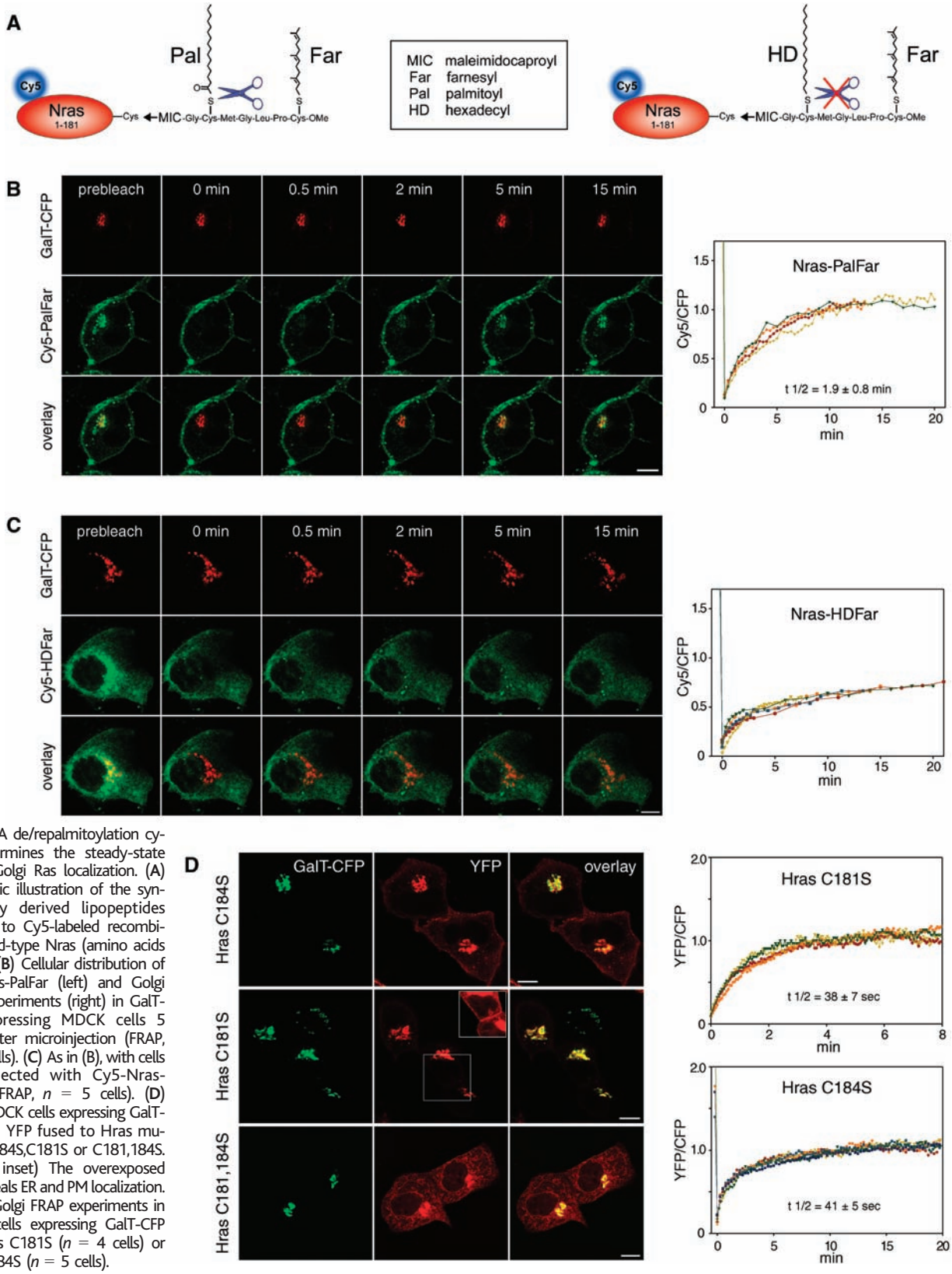

Fig. 2. A de/repalmitoylation cycle determines the steady-state PM or Golgi Ras localization. (**A**) Schematic illustration of the synthetically derived lipopeptides coupled to Cy5-labeled recombinant wild-type Nras (amino acids 1-181). (**B**) Cellular distribution of Cy5-Nras-PalFar (left) and Golgi FRAP experiments (right) in GalT-CFP–expressing MDCK cells 5 hours after microinjection (FRAP, $n = 4$ cells). (**C**) As in (B), with cells microinjected with Cy5-Nras-HDFar (FRAP, $n = 5$ cells). (**D**) (Left) MDCK cells expressing GalT-CFP and YFP fused to Hras mutants C184S,C181S or C181,184S. (Center inset) The overexposed area reveals ER and PM localization. (Right) Golgi FRAP experiments in MDCK cells expressing GalT-CFP and Hras C181S ($n = 4$ cells) or Hras C184S ($n = 5$ cells).

branes. A fusion of paGFP to farnesylated but not palmitoylated Hras C181,184S, which was selectively photoactivated in a restricted area of MDCK cells, indeed repartitioned to all membranes in less than a minute (fig. S5A). To inhibit protein palmitoylation, MDCK cells expressing GalT-CFP and YFP-Hras were incubated with 2-bromopalmitate (2BP) (*24*, *25*). The fluorescence recovery kinetic of YFP-Hras at the Golgi under these conditions was greatly reduced and did not reach a plateau on the time scale observed for untreated cells (Fig. 1C). Because trapping at the Golgi did not occur, we observed only a slow increase in Golgi fluorescence in the FRAP curves because of the unspecific accumulation of depalmitoylated but still farnesylated Ras in all membranes. In a control experiment, we verified that 2BP did not block endocytosis under the same conditions (fig. S5B).

To obtain an independent proof for the requirement of de/repalmitoylation for retrograde Ras trafficking, we applied a chemical-biological approach by using two different synthetically lipidated Nras proteins: a palmitoylated control protein (PalFar) and a hexadecylated protein (HDFar) with a noncleavable thioether bond that cannot undergo de/reacylation. The synthesis of these lipidated Nras proteins was achieved by coupling their respective lipopeptides to Cy5-labeled, C-terminally truncated, recombinant Nras (Fig. 2A). The PalFar hybrid protein resembles full-length Nras, except for the nonpeptide maleimidocaproyl linker, and has been shown earlier to interact properly with effector proteins and to have activity in pheochromocytoma cell (PC12) differentiation assays comparable to that of wild-type Ras (*26*). Indeed, the microinjected PalFar hybrid protein localized normally to PM and the Golgi and exhibited Golgi FRAP kinetics similar to those of YFP-Nras (Fig. 2B). Under the same conditions, the hexadecylated HDFar protein localized unspecifically to the entire membrane system and did not display restricted Golgi or PM localization, even 20 hours after injection (Fig. 2C). Specific Golgi recovery was not apparent in a FRAP experiment. Instead, the recovery was incomplete and biphasic, with only partial recovery on ER membranes colocalizing with the Golgi through lateral diffusion. These experiments show that retrograde PM-Golgi trafficking of Hras and Nras is mediated by depalmitoylation/repalmitoylation activities that act on Ras in different subcellular localizations. Together with the anterograde transport, which we further verified to occur via the secretory pathway (*8*) (supporting online text) (fig. S6, A to C), a cycle is generated that determines the specific PM and Golgi localization of Ras. This is in contrast to a model where the physicochemical properties of palmitate per se provide affinity for a particular membrane, allowing thermodynamic equilibrium binding. Without the de/reacylation cycle, palmitoylated Ras would incorrectly localize to any membrane compartment, as shown with the hexadecylated Nras protein.

Monopalmitoylation results in faster PM-Golgi exchange and increased partitioning to the Golgi apparatus. Because different kinetics of retrograde trafficking of monopalmitoylated Nras and dually palmitoylated Hras suggest that the speed of PM-Golgi exchange is dictated by the stability of palmitate attachment, we investigated if monopalmitoylated Hras mutants resemble Nras in their de/reacylation characteristics. Indeed, Hras C184S displayed a pronounced Golgi localization similar to that of Nras and more extensive than that of wild-type Hras (Fig. 2D). Hras C181S nearly exclusively localized to the Golgi, with only a little material at the PM and on the ER. In contrast, nonpalmitoylated Hras C181,184S did not exhibit a preference for specific membrane systems and appeared on all endomembranes including the Golgi. Golgi FRAP experiments revealed that both monopalmitoylated mutants exhibited rapid fluorescence recovery kinetics, with a $t_{1/2}$ of 38 s for Hras C181S and a $t_{1/2}$ of 41 s for Hras C184S (Fig. 2D). In agreement, earlier pulse-chase experiments have revealed a palmitate turnover six and four times faster for the respective mutants than for wild-type Hras (*27*, *28*). The nearly exclusive Golgi localization of the least stable palmitoylated Hras C181S suggests that palmitoylation is confined to the Golgi and is rapid relative to depalmitoylation and endomembrane repartitioning, because otherwise the protein would accumulate on endomembranes.

The de/reacylation cycle acts on N- and C-terminally palmitoylated peptide sequences. Both the minimal Hras membrane-targeting domain comprising the C-terminal nine amino acids of Hras [YFP-th (*9*)] and a geranylgeranylated Hras mutant exhibiting the C-terminal CAAX box of Rap1a (YFP-Hras-CLLL) (*29*) revealed Golgi fluorescence recovery kinetics similar to those of wild-type Hras (fig. S3, B and C). Thus, neither the Ras G domain nor specific farnesylation is required for retrograde Ras trafficking. We

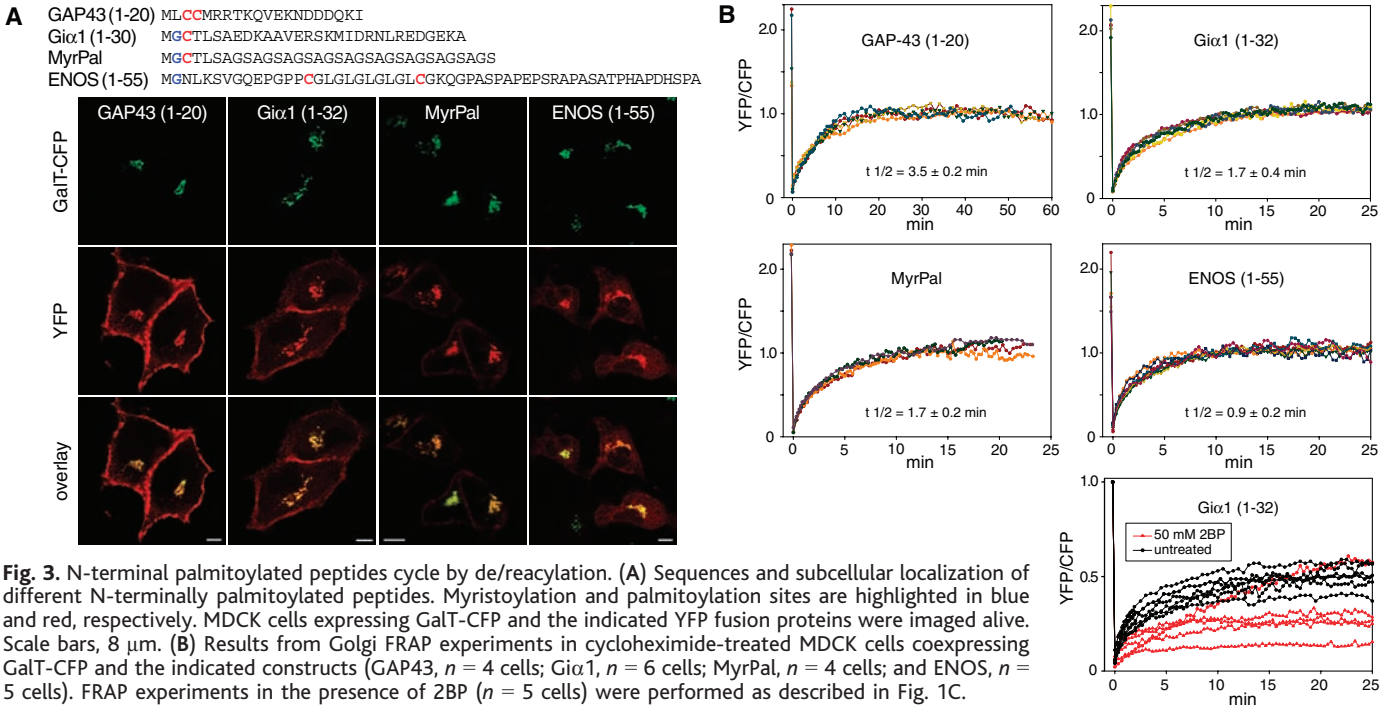

Fig. 3. N-terminal palmitoylated peptides cycle by de/reacylation. (**A**) Sequences and subcellular localization of different N-terminally palmitoylated peptides. Myristoylation and palmitoylation sites are highlighted in blue and red, respectively. MDCK cells expressing GalT-CFP and the indicated YFP fusion proteins were imaged alive. Scale bars, 8 μm. (**B**) Results from Golgi FRAP experiments in cycloheximide-treated MDCK cells coexpressing GalT-CFP and the indicated constructs (GAP43, n = 4 cells; Giα1, n = 6 cells; MyrPal, n = 4 cells; and ENOS, n = 5 cells). FRAP experiments in the presence of 2BP (n = 5 cells) were performed as described in Fig. 1C.

then investigated if N-terminal palmitoylated proteins are likewise controlled in their subcellular distribution by dynamic palmitoylation. A variety of these proteins have been reported to localize to the Golgi and PM, similar to C-terminally palmitoylated Ras (*30*). Four different palmitoylated N-terminal sequences were probed: GAP43-YFP (amino acids 1 to 20); Giα1-YFP (amino acids 1 to 32); MyrPal-YFP, an artificial myristoylated and palmitoylated sequence of 33 amino acids (*31*); and eNOS-YFP (endothelial NO-synthase, amino acids 1 to 55). All proteins displayed substantial Golgi staining and a varying extent of PM localization (Fig. 3A). Golgi FRAP experiments in the presence of cycloheximide revealed recovery kinetics similar to those observed with the different Ras isoforms and mutants. Moreover, inhibition of palmitoylation by 2BP resulted in a decreased fluorescence recovery (Fig. 3B). The FRAP kinetics again correlated with the extent of PM localization and thus might reflect the stability of palmitoylation. Dually palmitoylated GAP43, like Hras, was almost equally distributed between the Golgi and PM and recovered slowest ($t_{1/2}$ = 3.5 ± 0.2 min). Monopalmitoylated Giα1 and MyrPal, like Nras, recovered faster, and their PM localization was less pronounced than that of GAP43. ENOS displayed only little PM staining and recovered fastest. Although eNOS contains two palmitoylation sites, the fast kinetics might reflect inefficient acylation, because it has been shown earlier that the efficiency of acylation is dependent on the proximity of the reactive thiol to the membrane (*31*, *32*).

From these experiments, we propose a universal role for the de/reacylation cycle in targeting and dynamically distributing palmitoylated proteins to the PM and the Golgi. The lack of any apparent recognition sequences, together with the experiments with hexadecylated Nras and 2BP, strongly argues against the involvement of additional proteins facilitating membrane redistribution.

The lipid modification cycle initiates Golgi Ras activation. We investigated if retrograde Ras trafficking also accounts for net transport of PM Ras-GTP and thereby for active Golgi Ras after growth factor stimulation. A quantitative assay was developed to compare Ras activation dynamics in both compartments. In this assay, Ras-GTP is detected by its interaction with the Ras binding domain of Raf (RafRBD) through fluorescence resonance energy transfer (FRET) between YFP on Ras and dhcRed on RafRBD (Fig. 4A). Measuring FRET by the change in the fluorescence lifetime of the YFP donor with fluorescence lifetime imaging microscopy (FLIM), we can determine the molar fraction of Ras-GTP at each microscopically resolvable volume element (*33*). The selective occurrence of FRET between YFP and dhcRed upon Ras-RafRBD interaction, as measured by FLIM, has been validated by acceptor photobleaching (*34*) (fig. S7A). In agreement with previous experiments (*12*), this assay showed that Hras was rapidly and transiently activated at the plasma membrane after growth factor stimulus, whereas Golgi activation is delayed (by 10 to 20 min) and sustained (Fig. 4B). Importantly, the FLIM experiments demon-

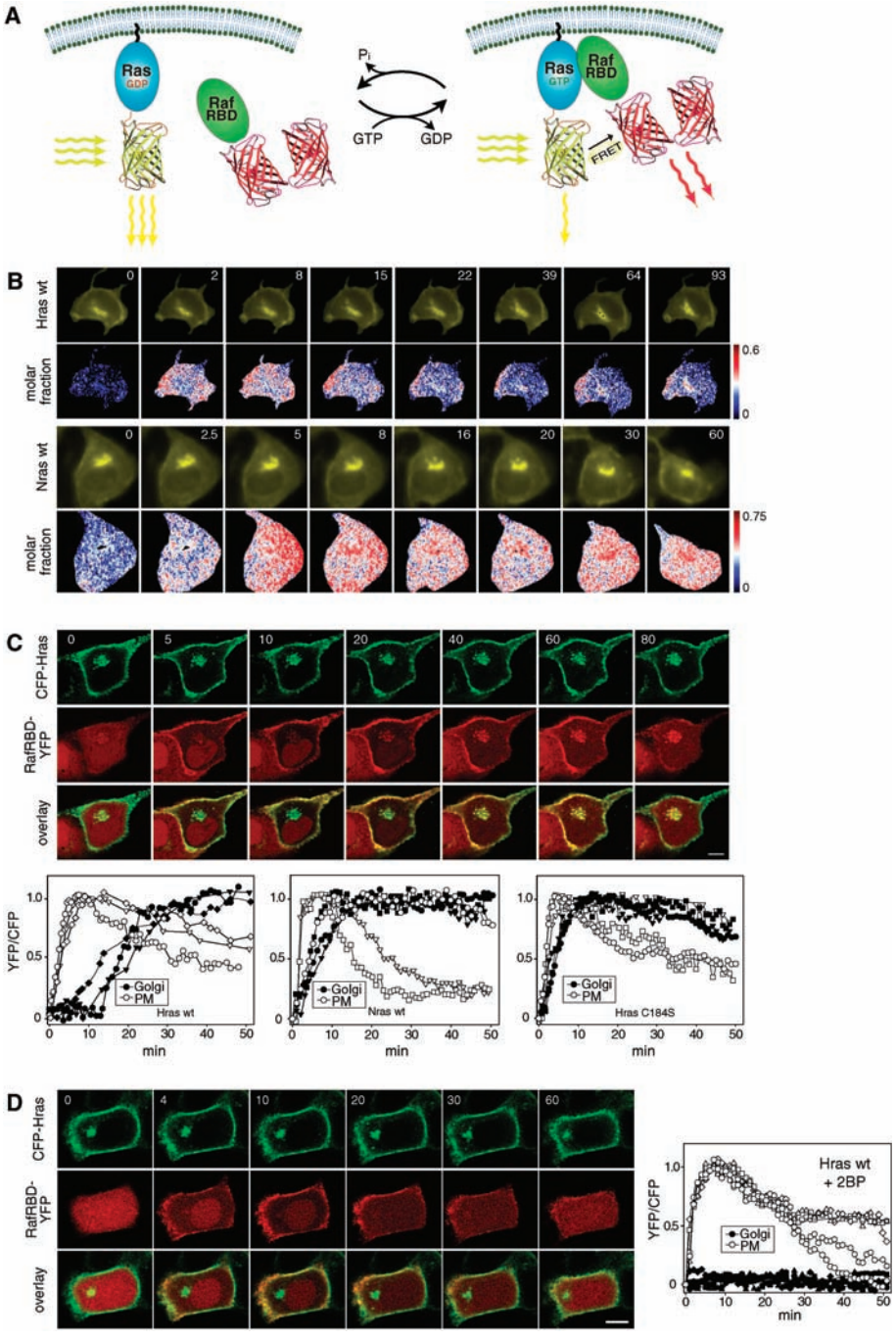

Fig. 4. The de/reacylation initiates Golgi Ras activation. (**A**) Schematic illustration of the FRET-FLIM–based Ras activation sensor. GDP, guanosine diphospate; RBD, Ras binding domain; GTP, guanosine triphosphate; P_i, phosphate. (**B**) FLIM-derived images of molar fractions of active Ras in MDCK cells coexpressing RafRBD-dhcRed and either YFP-Hras or YFP-Nras, after stimulation with 100 ng/ml EGF. Color bars: Calculated molar fraction of Ras-GTP. (**C**) (Top) EGF-induced membrane translocation of RafRBD-YFP in MDCK cells coexpressing CFP-Hras. (Bottom) Ratiometrical quantification of RafRBD-YFP translocation to the PM or the Golgi in MDCK cells cotransfected with wild-type CFP-Hras, wild-type CFP-Nras, or CFP-Hras C184S (n = 3 cells, represented by triangles, circles, and squares). Solid symbols, Golgi apparatus; open symbols, PM. (**D**) (Left) EGF-induced membrane translocation of RafRBD-YFP in 2BP-treated MDCK cells coexpressing CFP-Hras. (Right) Ratiometrical quantification of RafRBD-YFP translocation to the PM or the Golgi (n = 5 cells, each represented by different symbols). Solid symbols, Golgi apparatus; open symbols, plasma membrane.

strate that a large fraction of all Golgi Ras is activated after epidermal growth factor (EGF) stimulus. Hras activation kinetics were also monitored by tracking EGF-induced translocation of RafRBD-YFP to the PM or the Golgi in MDCK cells. Coexpression of CFP-Hras allowed ratiometric normalization to account for changes in local Ras concentration over time. PM Hras activation occurred with a $t_{1/2}$ of 2.9 ± 0.6 min, whereas Golgi Hras activation displayed a $t_{1/2}$ of 16.5 ± 4.0 min (Fig. 4C), resulting in a substantial delay of Golgi Hras activation ($\Delta t_{1/2}$ = 13.6 ± 4.0 min).

In contrast, activation of Nras or Hras C184S at the Golgi was detectable at markedly earlier time points and almost paralleled PM Ras activation in the FLIM assay (Fig. 4B and fig. S7C). Likewise, Golgi translocation of RafRBD-YFP occurred with a $\Delta t_{1/2}$ of only 2.3 ± 1.0 min or 1.9 ± 1.2 min in cells coexpressing the CFP fusions of Nras or Hras C184S, respectively (Fig. 4C and fig. S7B). Thus, the different time scales of retrograde PM to Golgi trafficking for the different palmitoylated Ras proteins correlate with their respective Golgi activation kinetics. We therefore investigated if inhibition of protein palmitoylation blocks Golgi Ras activation. Upon EGF stimulus, exclusive PM but no Golgi translocation of RafRBD-YFP was observed in cells coexpressing CFP-Hras that were pretreated with 2BP (Fig. 4D). Likewise, the fraction of active Golgi Ras was markedly reduced in the FLIM assay (fig. S7D). Taking together the findings that the faster retrograde Golgi trafficking of Nras or monopalmitoylated Hras correlates with their faster Golgi activation kinetics and that inhibition of retrograde trafficking blocks Golgi Ras activation, we conclude that a de/reacylation-driven transport of Ras-GTP from the PM accounts for initiation of Golgi Ras activity upon growth factor stimulation.

Discussion. A continuous cycle of de- and reacylation reactions accounts for the specific localization of palmitoylated Ras isoforms to the PM and Golgi apparatus and drives the rapid exchange of both protein pools. After depalmitoylation of fully lipid modified Ras, the still-farnesylated protein equilibrates between membranes and cytosol, allowing rapid redistribution to any cellular membrane. Stable membrane anchorage by repalmitoylation then occurs at the Golgi, where Ras is captured in the bulk-flow exocytic pathway redirecting the protein to the PM. This mechanism confers high accuracy in protein localization, because any spillover into other membrane compartments is prevented by the de/reacylation cycle that continuously resets the system. The precise localization is lost when the palmitate thioester is changed to a thioether bond that cannot undergo dynamic palmitoylation. The de/reacylation cycle not only occurs on Ras but acts on both N- and C-terminal palmitoylated peptide sequences. We therefore propose that the localization of peripheral membrane proteins is universally regulated by the de/reacylation cycle, provided that no other subcellular targeting mechanisms prevent access to this lipidation cycle. This mechanism could allow proper targeting of other palmitoylated proteins to distinct PM sites in polarized cells. These proteins will continuously have access to the sorting compartment and subsequently enter distinct post-Golgi trafficking pathways that could be specified by additional protein interactions (*35*). This localized bilayer trapping and release in different subcellular membrane compartments, governed by kinetic rather than thermodynamic factors (*36*), is a mechanism to generate compartmentalization of peripheral membrane proteins. Although these proteins are targeted into two separated membrane systems, the mechanism allows communication between both protein pools.

The lack of any apparent recognition signature for de/reacylation argues against the involvement of mammalian palmitoyltransferases (PATs) with unique sets of substrates, such as the recently reported yeast PATs Akr1 and Erf2/Erf4 (*37*, *38*). Alternatively, a very large family of similar specific PATs must exist. In a different scenario, palmitoylation might require a cysteine residue in membrane proximity, an environment that favors the formation of a thiolate ion in the cysteine to be acylated (*39*), and locally accessible acyl–coenzyme A (CoA). Transfer of the latter may be facilitated by acyl donor proteins (*40*) or by release of palmitoyl-CoA from acyl-CoA binding proteins, both on Golgi membranes.

A constitutive de/reacylation cycle accounts for transport of PM Ras-GTP to the Golgi after growth factor stimulation, and this is essential for initiation of Golgi Ras activation. This is distinct from but does not exclude a Golgi Ras activation mechanism involving the receptor tyrosine kinase (RTK)/Src/PLCγ1/Ca^{2+}/RasGRP1 pathway that was postulated to be separate from PM Ras activation through RTK/SOS (*14*). Because activation at the Golgi is prolonged in contrast to transient activation at the PM and because both compartments continuously exchange Ras through the de/reacylation cycle, an amplification through a positive feedback loop at the Golgi is likely to maintain local Ras activity after the initial triggering signal has vanished. A feedback mechanism for Ras activity involving Ras-GTP–induced exchange factor activation has been described (*41*).

By net transport of PM Ras-GTP, a cell can generate acute signaling at the PM in the context of receptor activation and initiate sustained signaling at the Golgi in a topologically separated membrane environment using the same signaling molecule. The stability of palmitate attachment, i.e., dual versus monopalmitoylation, thereby dictates the steady-state distribution and the speed of exchange of the PM and Golgi pools. This in turn allows fine-tuning of both the amplitude and the duration of signaling from each of the two compartments and thus determines which of the two protein pools will generate a stronger signaling output. Monopalmitoylated Nras displays a more pronounced Golgi localization, a faster retrograde PM-to-Golgi trafficking, and a several-fold shorter PM dwell time as compared to dually palmitoylated Hras. As a consequence, a larger fraction of Nras will exhibit prolonged activation patterns at the Golgi relative to Hras. This might cause Nras to couple more efficiently into Golgi-specific signaling pathways, as was recently shown for Erk1/2 activation in T cells (*13*). In addition, because of its fast palmitate turnover, Nras might have no access to the endosomal compartment, thereby adding another aspect of putative isoform-specific, compartmentalized signaling.

References and Notes

1. J. R. Silvius, *J. Membr. Biol.* **190**, 83 (2002).
2. J. F. Hancock, *Nature Rev. Mol. Cell Biol.* **4**, 373 (2003).
3. D. R. Lowy, B. M. Willumsen, *Nature* **341**, 384 (1989).
4. J. F. Hancock, A. I. Magee, J. E. Childs, C. J. Marshall, *Cell* **57**, 1167 (1989).
5. W. K. Schmidt, A. Tam, K. Fujimura-Kamada, S. Michaelis, *Proc. Natl. Acad. Sci. U.S.A.* **95**, 11175 (1998).
6. Q. Dai *et al.*, *J. Biol. Chem.* **273**, 15030 (1998).
7. J. F. Hancock, H. Paterson, C. J. Marshall, *Cell* **63**, 133 (1990).
8. E. Choy *et al.*, *Cell* **98**, 69 (1999).
9. A. Apolloni, I. A. Prior, M. Lindsay, R. G. Parton, J. F. Hancock, *Mol. Cell. Biol.* **20**, 2475 (2000).
10. J. E. Smotrys, M. E. Linder, *Annu. Rev. Biochem.* **73**, 559 (2004).
11. S. Roy, B. Wyse, J. F. Hancock, *Mol. Cell. Biol.* **22**, 5128 (2002).
12. V. K. Chiu *et al.*, *Nature Cell Biol.* **4**, 343 (2002).
13. I. Perez de Castro, T. G. Bivona, M. R. Philips, A. Pellicer, *Mol. Cell. Biol.* **24**, 3485 (2004).
14. T. G. Bivona *et al.*, *Nature* **424**, 694 (2003).
15. S. Torii, M. Kusakabe, T. Yamamoto, M. Maekawa, E. Nishida, *Dev. Cell* **7**, 33 (2004).
16. A. I. Magee, L. Gutierrez, I. A. McKay, C. J. Marshall, A. Hall, *EMBO J.* **6**, 3353 (1987).
17. K. Hirschberg *et al.*, *J. Cell Biol.* **143**, 1485 (1998).
18. H. Schroeder *et al.*, *Biochemistry* **36**, 13102 (1997).
19. R. G. Parton, K. Prydz, M. Bomsel, K. Simons, G. Griffiths, *J. Cell Biol.* **109**, 3259 (1989).
20. O. Rocks *et al.*, unpublished data.
21. G. H. Patterson, J. Lippincott-Schwartz, *Science* **297**, 1873 (2002).
22. D. Gerlich *et al.*, *Cell* **112**, 751 (2003).
23. J. R. Silvius, F. l'Heureux, *Biochemistry* **33**, 3014 (1994).
24. Y. Webb, L. Hermida-Matsumoto, M. D. Resh, *J. Biol. Chem.* **275**, 261 (2000).
25. D. Michaelson *et al.*, *J. Cell Biol.* **152**, 111 (2001).
26. B. Bader *et al.*, *Nature* **403**, 223 (2000).
27. J. Y. Lu, S. L. Hofmann, *J. Biol. Chem.* **270**, 7251 (1995).
28. Our FRAP experiments reveal a palmitate turnover 15 to 20 times faster than previously found in pulse-chase experiments. This discrepancy is most likely due to incomplete removal of radioactive material from the cell on the time scale of lipid turnover, resulting in substantial reincorporation of tritiated palmitate.
29. B. T. Kinsella, R. A. Erdman, W. A. Maltese, *Proc. Natl. Acad. Sci. U.S.A.* **88**, 8934 (1991).
30. M. J. Bijlmakers, M. Marsh, *Trends Cell Biol.* **13**, 32 (2003).
31. I. Navarro-Lerida, A. Alvarez-Barrientos, F. Gavilanes, I. Rodriguez-Crespo, *J. Cell Sci.* **115**, 3119 (2002).
32. A. ten Brinke *et al.*, *Biochem. J.* **361**, 663 (2002).
33. P. J. Verveer, F. S. Wouters, A. R. Reynolds, P. I. Bastiaens, *Science* **290**, 1567 (2000).

34. P. I. Bastiaens, I. V. Majoul, P. J. Verveer, H. D. Soling, T. M. Jovin, *EMBO J.* **15**, 4246 (1996).
35. A. D. el Husseini, D. S. Bredt, *Nature Rev. Neurosci.* **3**, 791 (2002).
36. S. Shahinian, J. R. Silvius, *Biochemistry* **34**, 3813 (1995).
37. A. F. Roth, Y. Feng, L. Chen, N. G. Davis, *J. Cell Biol.* **159**, 23 (2002).
38. L. Zhao, S. Lobo, X. Dong, A. D. Ault, R. J. Deschenes, *J. Biol. Chem.* **277**, 49352 (2002).
39. O. A. Bizzozero, H. A. Bixler, A. Pastuszyn, *Biochim. Biophys. Acta* **1545**, 278 (2001).
40. L. Xue, D. R. Gollapalli, P. Maiti, W. J. Jahng, R. R. Rando, *Cell* **117**, 761 (2004).
41. S. M. Margarit *et al.*, *Cell* **112**, 685 (2003).
42. We thank J. Ellenberg, J. Lippincott-Schwartz, I. Rodriguez-Crespo, M. R. Philips, J. Hancock, and H. T. McMahon for generously providing plasmids and A. Squire for technical help in microscopy. M.K. was supported by a fellowship of the Boehringer Ingelheim Fonds.

Supporting Online Material
www.sciencemag.org/cgi/content/full/1105654/DC1
Materials and Methods
SOM Text
Figs. S1 to S7
References and Notes

24 September 2004; accepted 10 December 2004
Published online 11 February 2005;
10.1126/science.1105654
Include this information when citing this paper.

Evolution of Oxygen Secretion in Fishes and the Emergence of a Complex Physiological System

Michael Berenbrink,[1,2]* Pia Koldkjær,[1] Oliver Kepp,[2]† Andrew R. Cossins[1]

We have reconstructed the events that led to the evolution of a key physiological innovation underpinning the large adaptive radiation of fishes, namely their unique ability to secrete molecular oxygen (O_2). We show that O_2 secretion into the swimbladder evolved some 100 million years after another O_2-secreting system in the eye. We unravel the likely sequence in which the functional components of both systems evolved. These components include ocular and swimbladder countercurrent exchangers, the Bohr and Root effects, the buffering power and surface histidine content of hemoglobins, and red blood cell Na^+/H^+ exchange activity. Our synthesis reveals the dynamics of gains and losses of these multiple traits over time, accounting for part of the huge diversity of form and function in living fishes.

Teleost fishes achieve neutral buoyancy by means of a gas-inflated swimbladder (*1*). This innovation removed constraints on pectoral and caudal fin structure (*2*), allowing the adaptive radiation of the life-styles, habitats, and morphologies in modern fishes. The subsequent evolution of an O_2 secretion mechanism to inflate the swimbladder removed the need to take in air through the esophagus at the surface, allowing colonization of new habitats such as the deep sea. The underlying physiology of O_2 secretion involves pH-sensitive "Root-effect" hemoglobins and an elaborate vascular arrangement known as the *rete mirabile* (Latin: wonderful network; plural, *retia mirabilia*).

Arterial blood passing through the capillaries of the gas gland in the swimbladder wall is acidified by release of lactic acid and carbon dioxide from gas gland cells (*3*). Low pH then causes a strong decrease in the O_2 binding capacity of Root-effect hemoglobins (Hbs) despite high oxygen tensions (*4*). The concomitant increase in physically dissolved O_2 is amplified by the *rete mirabile*, a tight bundle of arterial and venous capillaries running closely together in opposite directions, which provides a countercurrent exchange allowing diffusion of O_2 unloaded from Hb in the venous capillaries back into the arterial supply to the swimbladder. The ensuing buildup of high O_2 tensions then fills the swimbladder by diffusion, even against high hydrostatic pressures (*3*). The (alkaline or normal) Bohr effect of mammalian Hbs describes the acid-induced decrease in Hb O_2 affinity at alkaline to neutral pH. The Root effect differs from the Bohr effect in that acidification unloads O_2 from Root-effect Hbs even at O_2 tensions above atmospheric levels (*3*, *4*).

Teleosts deviate in two other important ways from the general pattern of vertebrate blood gas transport: They have Hbs with unusually low specific buffer values such that less acid is needed to elicit the Root effect (*5*), and they can use an isoform of the vertebrate Na^+/H^+ exchanger family (βNHE) to regulate the intracellular pH of red blood cells (*6*, *7*). Low Hb buffer values also mean that less acid need be shifted by the βNHE to modify red blood cell pH. Teleost Hbs also display some of the greatest (alkaline or normal) Bohr effects among jawed vertebrates (*5*).

There is currently no coherent explanation for the many advanced teleost groups that lack one or several of these various physiological traits. This picture is further complicated by the presence of elevated O_2 tensions in the eyes of many fishes (*8*). An ocular mechanism comprising a choroid *rete* works similarly to the swimbladder *rete* to increase physically dissolved O_2 and thereby supports the vigorous O_2 demand of the often avascular fish retina (*9*).

By taking advantage of the wide divergence of fishes and by integrating data from all levels of organization, we reconstruct on a vertebrate phylogeny the likely sequence of evolutionary events leading to the ability to secrete O_2. We support this analysis by identifying consistent patterns of secondary losses of several of these components in specific clades of advanced fishes, thereby characterizing factors that affect their maintenance.

Evolution of the Root effect and *rete mirabile*. In the absence of the acid-induced elevation of venous O_2 tension by the Root effect, the *rete* would shunt O_2 from the arterial supply directly to the venous drainage, bypassing the tissue. Thus, evolution of an O_2-permeable *rete* before the Root effect may conceivably be physiologically constrained (*retia*-only-with-Root hypothesis). We tested this hypothesis by first establishing the presence or absence of choroid and swimbladder *retia* in more than 50 selected vertebrate species and then reconstructing the evolution of these structures on a composite vertebrate phylogeny (*10*) (Fig. 1). The choroid *rete* evolved only once, some 250 million years ago. By contrast, swimbladder *retia* evolved independently in four major teleost groups (A, B, C, and D in Fig. 1) and were secondarily lost several times. The two earliest origins of swimbladder *retia* are found among the Elopomorpha (C) and Euteleostei (A) and can be dated back to 130 to 140 million years ago. Evolution of swimbladder O_2 secretion was followed by the invasion of a deep-sea habitat in Elopomorpha (C) and can be associated with modifications of the swimbladder for increased auditory sensitivity in Osteoglossomorpha (D) (*10*). In both groups, this was paralleled by significant adaptive radiations, as is evident from a substantial increase in extant species numbers relative to the respective sister groups without swimbladder O_2 secretion [771 versus 8 species for Albuliformes + Notacanthiformes + Anguilliformes versus Elopiformes, and 198 versus 8 species for Mormyroidea versus Notopteridae; $P < 0.05$ in both cases (amplified diversification test) (*10*)].

Next, we measured the Root effect in 49 of the species used for reconstruction of *rete*

[1]School of Biological Sciences, University of Liverpool, Crown Street, Liverpool L69 7ZB, UK. [2]Department of Animal Physiology, Humboldt Universität zu Berlin, Philippstraβe 13, D-10115 Berlin, Germany.

*To whom correspondence should be addressed. E-mail: michaelb@liv.ac.uk

†Present address: Molecular Biology, Max Planck Institute for Infection Biology, Schumannstr. 21/22, D-10117 Berlin, Germany.

An Acylation Cycle Regulates Localization and Activity of Palmitoylated Ras Isoforms

Oliver Rocks *et al.*

Science **307**, 1746 (2005);
DOI: 10.1126/science.1105654

Science (print ISSN 0036-8075; online ISSN 1095-9203) is published weekly, except the last week in December, by the American Association for the Advancement of Science, 1200 New York Avenue NW, Washington, DC 20005.